IOP Publishing Phys. Med. Biol. 65 (2020) 015017 (18pp) https://doi.org/10.1088/1361-6560/ab589a

Physics in Medicine & Biology

IPEM Institute of Physics and Engineering in Medicine

PAPER

Photodynamic therapy in 2D and 3D human cervical carcinoma cell cultures employing LED light sources emitting at different wavelengths

RECEIVED
19 June 2019

REVISED
11 November 2019

ACCEPTED FOR PUBLICATION
18 November 2019

PUBLISHED
13 January 2020

María E Etcheverry[1,2], Miguel A Pasquale[2], Cecilia Bergna[3], Carlos Ponzinibbio[3] and Mario Garavaglia[1,4,5]

[1] Facultad de Ciencias Exactas, Departamento de Física, Universidad Nacional de La Plata (UNLP), La Plata, Argentina
[2] Instituto de Investigaciones Fisicoquímicas Teóricas y Aplicadas (INIFTA) (CCT CONICET La Plata, Universidad Nacional de La Plata (UNLP), La Plata, Argentina
[3] Facultad de Ciencias Médicas, Cátedra B de Patología, UNLP, La Plata, Argentina
[4] Centro de Investigaciones Ópticas (CIOp) (CCT CONICET La Plata, UNLP y CIC), La Plata, Argentina
[5] Author to whom any correspondence should be addressed.

E-mail: garavagliam@ciop.unlp.edu.ar

Keywords: photodynamic therapy, LEDs, 2D and 3D HeLa cell culture, m-THPC, cervical intraepithelial neoplasias

Abstract

Light of different wavelengths can be used to obtain a more profitable outcome of photodynamic therapy (PDT), according to the absorption bands of the photosensitizer (PS). Low-grade cervical intraepithelial neoplasias (CINs) are superficial lesions that can be treated with light of shorter wavelength than red because a large light penetration depth in tissue is not necessary. We report a comparative investigation performed to evaluate the efficacy of light-emitting diodes (LEDs) of different wavelengths in the photodynamic treatment applied to both 2D and 3D HeLa cell spheroid cultures. The spheroids are utilized as a PDT dosage model, and cell viability is evaluated at different sections of the spheroids by confocal microscopy. Cells incubated with m-tetrahydroxyphenyl chlorin are illuminated with LED systems working in the low fluence range, emitting in the violet (390–415 nm), blue (440–470 nm), red (620–645 nm) and deep red (640–670 nm) regions of the light spectrum at various exposures times (t_I) comprised between 0.5 and 30 min. PDT experiments performed on both 2D and 3D cell cultures indicate that the PDT treatment outcome is more efficient with violet light followed by red light. Dynamic data from the front displacement velocity of large 2D-quasi-radial colonies generated from cell spheroids adhered to the Petri dish bottom as well as the evolution of the 3D growth give further insight about the effect of PDT at each condition. Results from 3D cultures indicate that the penetration of the violet light is appropriate to kill HeLa cells several layers below, showing cell damage and death not only in the outer rim of the illuminated spheroids, where a PS accumulation exists, but also in the more internal region. Results indicate that violet LED light could be useful to treat CINs involving superficial dysplasia.

1. Introduction

Photodynamic therapy (PDT) is an emerging, minimally invasive therapeutic procedure that can selectively destroy the tumor tissue with photosensitizers activated by specific wavelength light in the presence of oxygen (Dougherty *et al* 1998). Upon light absorption, the photosensitizer initiates photochemical reactions that result in the formation of reactive oxygen species (ROS), particularly singlet oxygen ($^1O_2$), which can cause significant cytotoxicity leading to the decrease of mitochondrial activity (Castano *et al* 2005, Jarvi *et al* 2012) and the increase of the proportion of cells with DNA fragmentation (Nonaka *et al* 2010). It is widely known that the activation light is one of the primary components of PDT, and thus the choice of light sources is crucial for PDT studies. Additionally, fluence rate may be critical to modulate the PDT mechanism and its outcome (Allison *et al* 2010, Allison and Moghissi 2013, Hartl *et al* 2015). Thus, with high rates of light delivery, PDT occurs favoring necrosis pathways and immune stimulation (Oleinick and Evans 1998). If fluence is too high, singlet

oxygen may be depleted, but extreme rates are not likely to be achieved in the clinic. Contrarily, low fluence rates most probably push PDT into the apoptotic pathways (Agarwal *et al* 1991). This may be critical to avoid robust normal tissue reaction as may occur when damaged tissue releases cytokines and other immune modulators that increase inflammation and swelling. Conceivably, at low illumination rates, a highly reactive PS such as m-tetrahydroxyphenyl chlorin (m-THPC) (Abrahamse and Hamblin 2016) may become more selective and less toxic to normal tissue via favoring apoptosis pathways. The m-THPC photosensitizer is a reduced porphyrin developed in the 90's that has a stronger absorption peak in the spectral UV/violet zone than in the red one. It possesses a proven high antitumor activity and good selectivity for tumor tissue (Bonnett *et al* 1989, Senge and Brandt 2011) and shares many characteristics of an ideal sensitizer (Horrobin 1994). A considerable number of papers reported the utilization of m-THPC for *in vitro* experiments with different cells, *in vivo* tumor models and clinical applications (Senge and Brandt 2011). It is currently approved by the U.S. Food and Drug Administration (FDA) and the European Medicines Evaluation Agency (EMEA) for local palliative treatment of advanced head and neck cancers (Lorenz and Maier 2009, Senge and Brandt 2011).

The amount of light deposited and its distribution in the treated sample are important characteristics of PDT. They are determined by both the light source characteristics and the sample optical properties (Potter 1986, Foster *et al* 1993, Sandell and Zhu 2011, Baran and Foster 2012). The latter are influenced by the concentration distribution of photosensitizer and oxygen in the sample, which in the case of a tissue depends on the blood perfusion and on the blood composition (Penjweini *et al* 2016). Similarly, the distribution of oxygen is altered by the photodynamic process, which consumes oxygen and may alter blood flow. Finally, the distribution of photosensitizer may change as a result of photobleaching, the photodynamic destruction of the photosensitizer itself (Lacowicz 2006). Light penetration through a tissue plays a key role in the PDT outcome, thus the optical properties of a large number of tissues, mucosa, cavities and organs have been reviewed (Jacques 2013). Moreover, Monte Carlo-based modeling has been employed to analyze the effect of the light wavelength as well as the light beam width on tissue penetration (Ash *et al* 2017).

From a physical point of view, the PDT dose is defined, on the tissue surface, as the product of drug concentration and total incident light dose; while to account for the reduction of the dose with the depth into the tissue, the attenuation of light is considered (Potter 1986, Boyle and Potter 1987). In tissue regions far from light sources, the fluence rate decays exponentially (van de Hulst 1980) and the effective light penetration can be evaluated (van de Hulst 1980, Martínez Abaunza *et al* 2005). For a wavelength approaching violet, a smaller light penetration than that for red has been reported (Etcheverry *et al* 2018). It is known that upon surface illumination the fluence rate-depth dependence exhibits a peak just below the surface limit, and it only becomes a decreasing exponential at certain depth (Wilson and Patterson 2008).

Different types of illumination sources have been proposed for photodynamic treatment and diagnosis (Enk and Levi 2012, Hatakeyama *et al* 2013, Finlay and Darafsheh 2016). Among them, LEDs have some advantages, since they are inexpensive, less hazardous, thermally nondestructive, and readily available. Nowadays, several papers have evaluated the PDT antitumor effect using various LED light wavelengths applied to *in vitro* and *in vivo* studies (Babilas *et al* 2006, Dias Ribeiro *et al* 2010, Hatakeyama *et al* 2013, Helander *et al* 2014, Novak *et al* 2016, Jamali *et al* 2018). Other previous papers in which non-LED sources were employed have proposed a methodology for choosing the appropriate illumination wavelength based on the action spectrum of the photosensitizer (Moan and Sommer 1984, Moan *et al* 1989, Moan *et al* 1992). Moreover, green light has been employed in clinical PDT with δ-aminolevulinic acid sensitization of facial keratoses and compared with red light (Fritsch *et al* 1997). In this work the effectiveness of both lights has been demonstrated to be comparable, although violet light exhibited fewer side effects. In this vein, another work has indicated that 514 nm green light utilized in PDT with Photofrin II had the potential to cure superficial cancer in the esophagus and bronchi with the same statistically significant efficacy as 637 nm red light, but in the case of the esophagus, green light prevented deep tissue damage (Grosjean *et al* 1998). This is reflected in the decrease in the risk of oesophagus wall perforation and complications. More recently, the use of 400 nm light PDT with δ-aminolevulinic acid for the treatment of basal cell carcinoma in patients with Gorlin syndrome has been reported. The authors have suggested that 400 nm light appears to be less painful and equally effective to 635 nm light (Maytin *et al* 2018).

Cervical cancer is the second most common neoplastic disease in women. It is associated with human papillomavirus (HPV), particularly HPV 16 and 18, which are responsible for precancerous cervical intraepithelial neoplasia (CIN) and invasive cancer (Walhoomers *et al* 1999). CINs are superficial lesions classified according to the dysplasia grade and extension of the neoplasia along the epithelium. This classification goes from CIN 1, involving a mild dysplasia confined to 1/3 of the epithelium, to CIN 3, which comprises a severe dysplasia involving more than 2/3 of the epithelial thickness (World Health Organization 2014).

On the other hand, spheroids, i.e. tridimensional aggregates of cells coming from one or several cell clones, have been utilized in PDT experiments (Dubessy *et al* 2000, Finlay *et al* 2004, Madsen *et al* 2006, Evans 2015, Gaio *et al* 2016, Pereira *et al* 2017, Mohammad-Hadi *et al* 2018). This model better mimics the tridimensional tumor microstructure and some of their properties, and shows oxygen, pH and nutrient gradients inducing a necrotic

area in the center of the spheroid. The response of intermediate-size (~500 μm-diameter) multicellular tumor spheroids to a given dose of PDT depends critically on the illumination fluence rate at which the therapy is administered (Foster *et al* 1993, Angell-Petersen *et al* 2006). Spheroids were found to be less sensitive to PDT than monolayers and, as the spheroid size increased, the sensitivity to PDT decreased (Mohammad-Hadi *et al* 2018). The concept of photochemical oxygen consumption initially developed in spheroids was later confirmed in a preclinical tumor system (Angell-Petersen *et al* 2006, Morales Cruzado and Vázquez-Montiel 2011).

In this work we evaluate the efficiency of PDT applied to both 2D and 3D HeLa cell spheroid cultures employing m-THPC as photosensitizer and LED lights emitting in the range 390–415 nm (violet), 440–470 nm (blue), 620–645 nm (red), and 640–670 nm (deep red). The PDT efficiency for the different lights was compared with what might be expected from the fluorescence-excitation spectrum of m-THPC bound to HeLa cells. The growth dynamics of 2D and 3D colony regions were evaluated for untreated and PDT-treated with either violet or deep red light adhered cell spheroids, and PDT efficiency and complementary information about the treatment were assessed. Confocal microscopy was used to determine whether violet light penetrated sufficiently to kill HeLa cells several layers below the spheroid apex. The results from the experiments employing both 2D and 3D HeLa cell spheroids were analyzed for determining whether violet light was suitable for the photodynamic treatment of CINs, as has been reported for other superficial neoplastic diseases.

2. Materials and methods

2.1. Cell culture

HeLa cells from human cervical adenocarcinoma were obtained from Asociación Banco Argentino de Células (ABAC) at passage 48. For all experiments, cultures were maintained between ten passages (50–60). The morphological and growth characteristics are consistent with those indicated by the American Type Culture Collection (ATCC) as we described in previous publications (Huergo *et al* 2012, Muzzio *et al* 2014). Cells were grown as monolayers in RPMI (Gibco) supplemented with 10% fetal bovine serum (FBS) (Natocor, Argentina) in a humidified incubator with 5% CO_2 and 95% air at 37 °C (Isotemp Fisher Scientific). The cells were subcultured every 3 d until an adequate number of cells were obtained for the study. After reaching approximately 80% density, the cells were trypsinized, seeded (10^5 cells) in sterile polystyrene Petri dishes 3.5 cm in diameter (Grinner Bio-One) and incubated for about 24 h prior to PDT experiments. All procedures for the maintenance of cells and the preparation of cultures were performed under sterile conditions using a laminar flow.

2.2. Spheroid of HeLa cells

A suspension of HeLa cells (2×10^5 cells ml^{-1}) was poured into a bacteriological Petri dish 10 cm in diameter exhibiting poor mammalian cell adhesion. Under these conditions, spheroids are formed in a week. Then the spheroids were individually selected and collected with a micropipette and seeded in an adherent capsule with fresh culture medium, and left overnight in the incubator to get adhered to the substrate before incubating with the photosensitizer and performing the photodynamic treatment.

2.3. Light sources

LED systems consisting of 1W LED mounted on a platform 15 cm above the Petri dishes (figure 1(a)) with LEDs emitting in the range 390–415 nm (violet), 440–470 nm (blue), 620–645 nm (red) and 640–670 nm (deep red), hereafter named LED A, B, C and D, respectively, were used to activate the photosensitizer. LED-based devices were constructed with high power 1 W LEDs from Epileds, Taiwan. These LEDs were chosen because they are easily commercially available and allow a comparative study on the basis of the overlapping of their emission spectrum and the absorption bands of the employed photosensitizer. LED-based sources were characterized employing a spectrometer AvaSpec-ULS3648-USB2-UA-25 provided with an optical fiber FC-UVIR200-2.

The characteristic parameters from each LED-based source are depicted in table 1. Irradiance values are calculated at 15 cm from the source. Considering our measurement errors, each LED presents a homogenous illumination of the Petri dish bottom surface (figures 1(a) and (b)). The large relative difference in illuminance values between each source is due to the electromagnetic wavelength sensitivity for photopic vision according to the Commission Internationale de l'Eclairage (CIE, Publication 18.2, 1983).

2.4. Photosensitizer

The m-THPC photosensitizer (Foscan®, from Scotia Pharmaceuticals Ltd) was used in the experiments. The absorption and fluorescence spectra of the m-THPC bound to cells (figure 2) were obtained from a cell suspension of 10^5 cells ml^{-1} in phosphate buffered saline (PBS). These cells were previously incubated in a T-25 culture flask (Greiner Bio-One) with m-THPC at 2 μg ml^{-1} solution in RPMI medium for 24 h, and then scraped with a Falcon^R scraper after washing trice with ice-cold PBS. The absorption spectrum of the m-THPC was also obtained from both a solution in PBS and a solution in methanol (figure 2). It is worth noting that, in

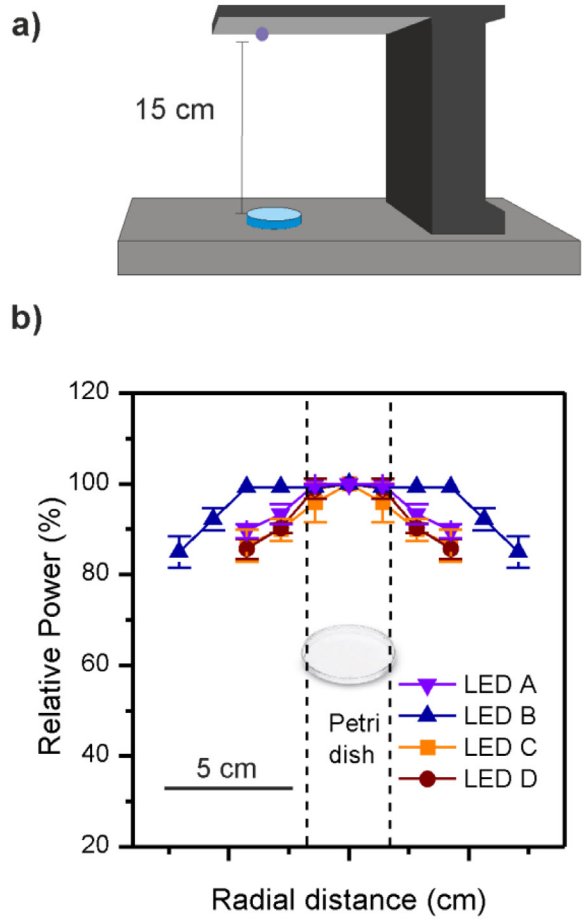

Figure 1. (a) Scheme of the arrangement of the LED-based illumination system used in PDT. (b) Relative power percentage for the different LEDs used in the experiments. The relative power is homogeneous on the substrate surface at 15 cm from the light source.

Table 1. Characteristics of the LEDs. The wavelength range with irradiance larger than 20% of the maximum, the maximum irradiance, the illuminance and the photon flux are listed.

LED	Emitting range (nm)	Irradiance (μW cm^{-2}) at the maximum	Illuminance (lux; lm m^{-2})	Photon flux (cm^{-2})
A	390–415	12.41	11.37	7.0
B	440–470	12.92	234.1	17.5
C	620–645	12.24	467.0	12.0
D	640–670	12.89	173.5	14.0

PDT applications, the light needs to penetrate the tissue for activating the photosensitizer upon absorption. A smaller penetration of light in the violet region than in the red one has been reported (Etcheverry *et al* 2018). For the treatment of early cases of cervical uterine carcinoma, the light must be capable of traversing about 250 μm to reach abnormal cells at the epithelium (Ghosh *et al* 2015), as can be appreciated from the scheme in figure 2(b). The tissue comprised different types of cells: superficial, middle zone and basal cells (Martínez Abaunza *et al* 2005).

For PDT experiments, the cultures were incubated with the photosensitizer in RPMI maintenance medium containing 2% FBS, thus cells are maintained in a relatively low living metabolic state, at concentrations of the photosensitizer, $C_p = 0.05, 0.25, 0.1, 0.5$ and 2 μg ml^{-1}. These solutions were obtained from a 100 μg ml^{-1} stock solution in methanol.

Complex molecules such as m-THPC exhibit broad absorption/emission bands mainly due to the distribution of vibration and rotation energies at ambient temperature, although these bands depend on the interaction of the molecule with the environment (Lacowicz 2006).

2.5. Photodynamic therapy (PDT)

After the appropriate growth of 2D or 3D cell cultures, the culture medium supplemented with 10% FBS was removed, and the photosensitizer at the corresponding concentration C_P in fresh maintenance medium was

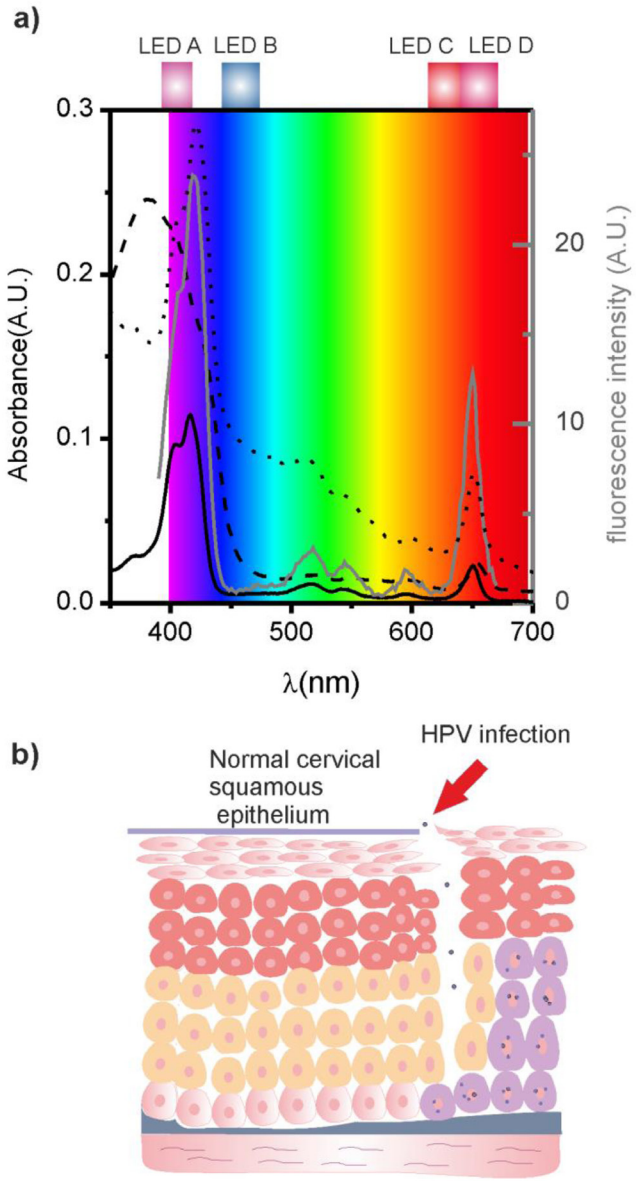

Figure 2. (a) Absorption spectra of m-THPC in PBS at 4 μg ml^{-1} (dashed black line), in methanol at 4 μg ml^{-1} (solid black line) and bound to HeLa cells (dotted black line) overlapped with the visible light spectrum. The excitation-emission fluorescence spectrum for m-THPC bound to HeLa cells (dotted gray line) is also included. The different LED light emission ranges employed in the experiments are indicated by colored boxes. (b) Scheme of a low-grade squamous intraepithelial lesion (CIN1), comprising 1/3 (about 80 μm) of the lower epithelial region.

incorporated. Then cell cultures were incubated with the photosensitizer for a certain deep interval (3–24 h) and finally the cells were exposed to different LED sources, and different energy densities, according to an exposure time (t_1) of 30, 20, 15, 8, 4, 2, 1 and 0.5 min, employing the experimental arrangement shown in figure 1(a).

2.6. Analysis of cell metabolism (MTT assay)

Phototoxicity was assessed by employing thiazolyl blue tetrazolium bromide (MTT) from Life Technologies, measuring the formazan product after 6 and 24 h post-illumination. The culture medium was replaced by a new one containing MTT solution (0.5 mg ml^{-1} in RPMI growth medium). Cells were incubated in the presence of the MTT solution for 3 h at 37 °C. Subsequently, the culture medium was completely removed, and the formazan products were solubilized by adding 1 ml of DMSO to each capsule. This solution was poured into a 96-well culture plate, and the absorbance was measured at 570 nm by a plate reader (Genios Pro). Results were expressed as relative absorbance referred to a culture without illumination. Measurements were repeated three times, and the mean value and its standard error were reported for each condition.

2.7. TUNEL assay

Apoptotic cell death induced 1 h and 3 h after PDT was confirmed by TUNEL (Terminal deoxynucleotidyl transferase-mediated dUTP nick-end labeling) assay employing the *in situ* Cell Death Detection Kit from Roche (Cat. No. 12 156 792 910) and following the manufacturer's instructions.

Briefly, HeLa cells seeded on coverslips were fixed for 20 min in paraformaldehyde at 4 °C, permeabilized for 2 min with Triton X-100 (Sigma-Aldrich) and incubated for 1 h with TUNEL reaction mixture at 37 °C. After washing with PBS, preparations were analyzed. TUNEL-positive nuclei were counted in 8 randomly selected microscopic fields per sample, and the result expressed as a percentage of the total nuclei counted. At least 1500 nuclei were counted on each sample.

2.8. Acridine orange and propidium iodide (AO/PI) assay

After their PDT treatment HeLa cell spheroids were stained with acridine orange (50 μl of 0.01% AO in PBS) and propidium iodide (30 μl of 50 μg ml^{-1} PI in PBS) and analyzed by an Olympus BX51 fluorescence microscope with blue filter (excitation: 480/20, emission: 510 nm). Furthermore, other stained cell spheroids were analyzed with a Confocal Laser Spectral Microscope Leica TCS SP5 equipped with seven lines of laser, AOTF (Acousto-Optic Tunable Filter), AOBS (Acousto-Optical Beam Splitter) and tandem scanning system SP5.

2.9. Dynamics of 2D and 3D HeLa cell cultures

3D spheroids prepared as indicated above were incubated in maintenance medium containing the photosensitizer for 3–24 h before the photodynamic treatment. The colony growth pattern follow-up started after the spheroid adhesion onto the Petri dish, before PDT illumination.

The dynamics of both the 2D colony/medium and the inner central 3D cluster/2D colony interfacial regions were studied. For this purpose, sequential images of colony patterns, from both the 2D and the 3D colony regions, were recorded utilizing a Nikon DS-Fi1-U2 digital camera coupled to a Nikon TS100 phase-contrast inverted microscope with a CFI flat field ADL 10X objective at a resolution of 0.88 μm/pixel. Colony fronts were manually traced from computer screen images using a Wacom graphic tablet with a tracing error on the order of the pixel. The follow-up of colony growth patterns was extended for about 7 d. The average radius of the 2D spreading colony border and the inner 3D growth were determined by in-lab developed software as has been more extensively reported (Huergo *et al* 2011, 2014).

3. Results

3.1. Cell death quantification in 2D HeLa cell cultures

3.1.1. MTT assay in 2D HeLa cell cultures

The efficiency of the PDT employing LED light sources with different wavelengths was assessed by evaluating the absorbance of the formazan produced by living cells, 24 h after the treatment with t_I in the range 0–20 min and C_p in the range 0.05–2 μg ml^{-1} (figures 3 and 4). For $C_p = 2$ μg ml^{-1} (figure 3(a)) cell viability decreases to a minimum value close to 0.1 at $t_I = 8$ min, irrespective of the light wavelength, although for both LED A and LED D this minimum is reached at t_I close to 1 min, while for LED B and LED C this t_I is 8 and 4 min, respectively. Thus, the decay in the viability is more abrupt for light of LED A and LED D than for light of LED C and B; the latter being the less effective light source.

On the other hand, for $C_p = 0.5$ μg ml^{-1} (figure 3(b)) and $t_I = 8$ min cell viability reaches 0.1 only for LED A. For LED B, C and D, cell viability results in 0.8, 0.45 and 0.25 respectively.

Considering the above results, we chose the LED A and D as they resulted in more effective PDT, and evaluated the effectiveness of the treatment employing C_p either higher or smaller than 0.5 μg ml^{-1} in order to better depict the effect of the wavelength at different energy densities (figure 4). Accordingly, we used t_I of 20, 15, 12, 8, 4 and 2 min. Thus, for $C_p = 1$ μg ml^{-1} (figure 4(a)) and for 0.003 J cm^{-2} ($t_I = 4$ min) only the light of LED A reaches the minimum value of 0.1 in the relative absorbance. Furthermore, for $C_p = 0.05$ μg ml^{-1} (figure 4(b)) only LED A appears to be useful to kill cells.

Data from MTT assays for different light wavelengths and C_p (figures 3 and 4) plotted as the relative absorbance (fraction of surviving cells) as a function of t_I give curves resembling exponential decay functions. Thus, based on the linear quadratic irradiation model (Brenner *et al* 1998), the experimental data can be fitted to quantify the photodynamic effect for different wavelengths, employing the following equation that considers the exponential regime only:

$$S = \exp(-\alpha t_I) \tag{1}$$

where S is the fraction of surviving cells; α is a constant and t_I is the illumination time. The term in the exponential is an indication of the photodynamic dose ($D = \alpha t_I$).

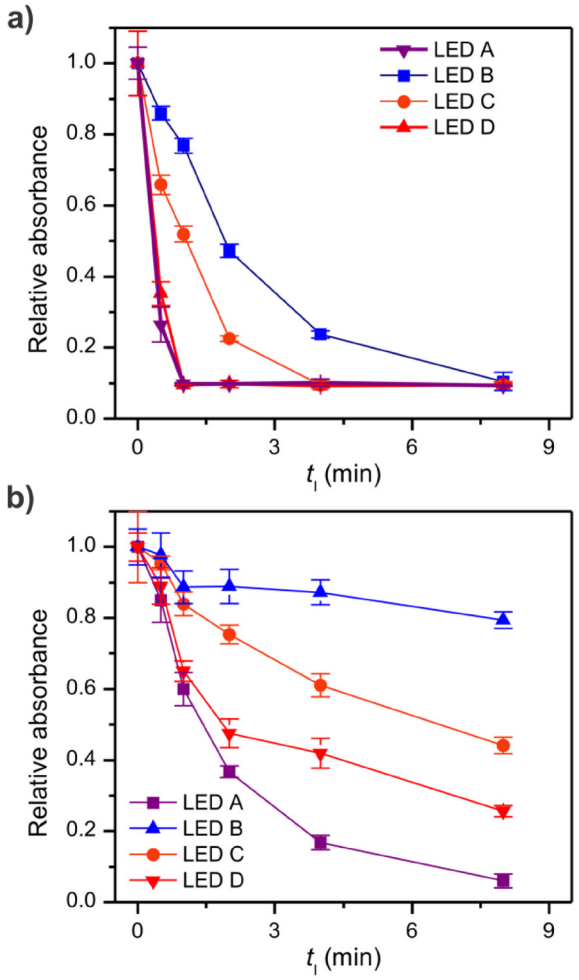

Figure 3. MTT assay for 2D HeLa cell cultures 6 h after PDT with different t_I: (a) $C_p = 2\ \mu g\ ml^{-1}$ and (b) $C_p = 0.5\ \mu g\ ml^{-1}$. Viability is expressed as relative absorbance, and the standard error is included for three experiments at each condition. Light source emitting in the range 390–415 nm (LED A) appears to be the most efficient source.

Following the above simple equation, values of α of $5\ min^{-1}$, $0.49\ min^{-1}$, $0.96\ min^{-1}$ and $4.4\ min^{-1}$ for LED A, B, C and D, respectively, were obtained from data depicted in figure 3(b).

3.1.2. TUNEL assay

TUNEL assay was employed to detect apoptotic cell death for both LED A and D, $C_p = 0.5\ \mu g\ ml^{-1}$ and different t_I (4, 6 and 8 min). For each condition, samples were visualized at 1 h and 3 h post-illumination (figures 5(a) and (b)). Unfortunately, the observation at longer times was not possible due to the detachment of cells after the photodynamic treatment, particularly for the longest t_I.

Data indicate that for both LED sources the apoptotic index (AI = 100 (apoptotic cells/ total number)), increases monotonically irrespective of the time of observation, either at 1 or 3 h post-illumination. For the same t_I, the AI is larger for cell cultures illuminated with LED A in comparison with LED D, irrespective of the observation time (1 or 3 h post-illumination).

For LED A the AI, 1 h post-illumination, increases from about 5% to 10%, and to 55% for $t_I = 4, 6$ and 8 min, respectively. In contrast, for LED D and 1 h after illumination, the AI remains constant and close to 5% for either $t_I = 4$ min or $t_I = 6$ min. Subsequently, this index increases up to about 30% for the longest t_I.

On the other hand, when cultures were observed 3 h after treatment, the AI for LED A increases from about 10% for $t_I = 4$ min to approximately 20% for $t_I = 6$ min and 80% for $t_I = 8$ min. In the case of LED D, the AI, at all t_I employed, is about half of that obtained for LED A.

Following one-way analysis of variance (ANOVA), further insight was obtained by comparing the mean of AI data obtained from illumination with the different t_I and each wavelength at either 1 or 3 h post-treatment. Fisher's least significant difference (LSD) test and $p < 0.05$ were employed. Significant differences were observed between LED A and D only for $t_I = 8$ min irrespective of the observation time, as indicated by the asterisk in figure 5.

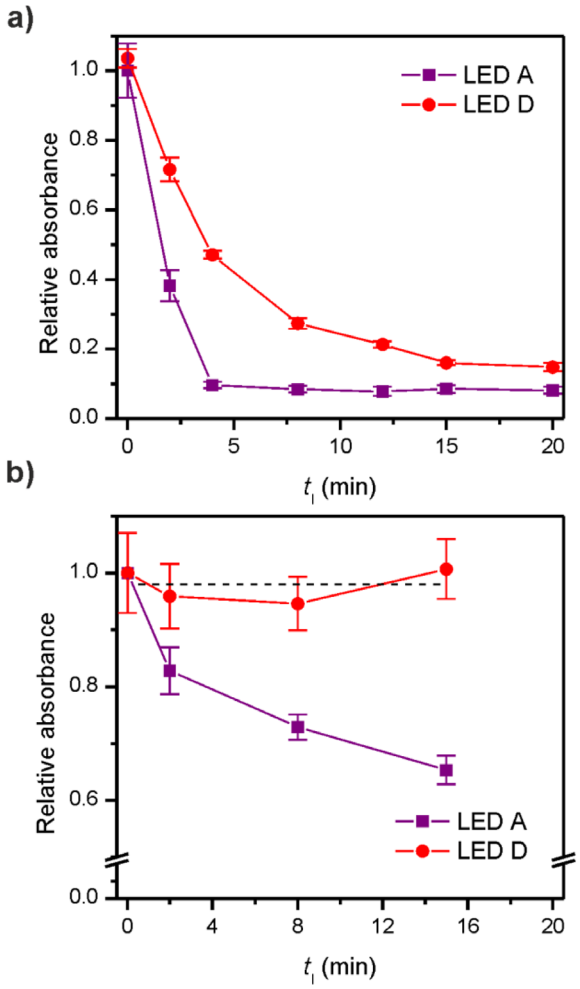

Figure 4. MTT assay for 2D HeLa cell cultures 6 h after PDT with different t_I: (a) $C_p = 1\ \mu g\ ml^{-1}$ and (b) $C_p = 0.05\ \mu g\ ml^{-1}$, employing LED A and D sources. Viability is expressed as relative absorbance, and the standard error is included for three independent experiments at each condition. For the minimum photosensitizer concentration LED D is unable to produce the photodynamic effect.

The overall data indicate that the increase in the proportion of apoptotic cells after PDT with increasing t_I correlates with MTT data, irrespective of the illumination light wavelength, i.e. either LED A or LED D.

3.2. Cell spheroids

Cell spheroids prepared as described in the experimental section were transferred to a Petri dish with fresh growth medium and left overnight to attain adhesion to the bottom. Then they were incubated with the photosensitizer in maintenance medium and illuminated with LED A or LED D and different t_I. We performed PDT experiments employing spheroids to study differences in the outcome in a more realistic situation. The dynamics of both 2D and 3D colonies generated by spheroids and followed by measuring the evolution of the average colony radius were analyzed to obtain complementary information about the PDT treatment outcome. Furthermore, spheroids were utilized to semiquantitatively describe the dosage during PDT.

3.2.1. Cell death induced by PDT in cell spheroids.

The penetration of the photosensitizer into the 3D HeLa cell spheroid was measured by fluorescence microscopy after incubation with 1 $\mu g\ ml^{-1}$ m-THPC in maintenance medium for 24 h. The red fluorescence of m-THPC is observed. A larger concentration of m-THPC at the spheroid border can be inferred from the fluorescence pattern (figure 6(a)), in consonance with results reported recently by other authors (Finlay *et al* 2004). For the conditions employed in our work, a large red fluorescence can be seen even inside the spheroid. This observation allows us to suppose that the m-THPC concentration is not a limiting factor.

Acridine orange and propidium iodide fluorescence visualization was used to assess cell death after different PDT conditions (figures 6(b) and (c)). Green staining indicates live cells and orange-stained cells are indicative of dead cells. Thus, cell viability was significantly lower, 24 h post-illumination, in spheroids treated with LED

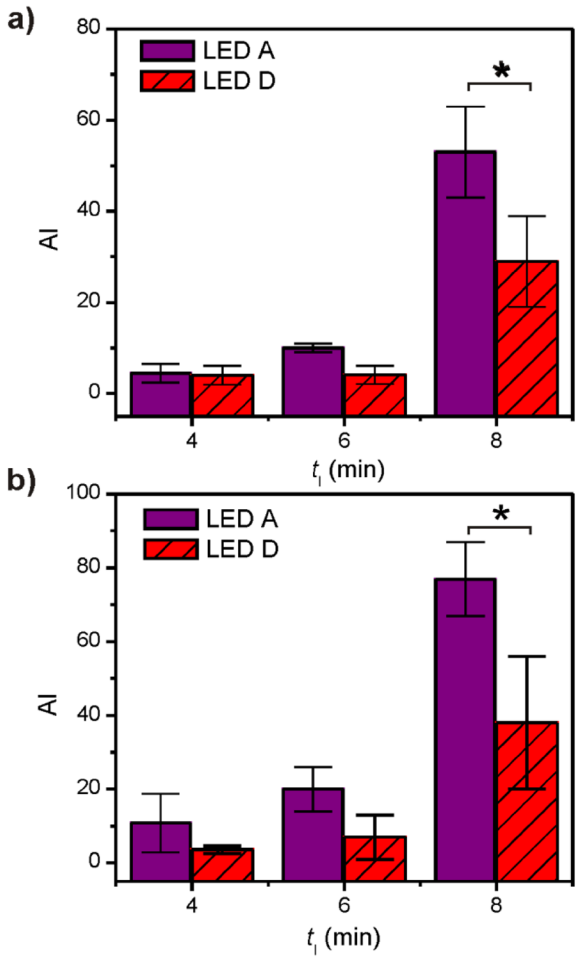

Figure 5. Apoptotic index (AI) versus illumination time from TUNEL assay of HeLa cell cultures illuminated with LED A and D for $t_I = 4, 6$ and 8 min as indicated. (a) Treated cultures observed at 1 h and (b) 3 h after illumination. Experiments were run with $C_p = 0.5\ \mu g\ ml^{-1}$.

A compared to LED D for the same photosensitizer concentration ($C_p = 1\ \mu g\ ml^{-1}$) and t_I (2 min and 12 min) (figure 6).

In addition, a significant difference in the colony pattern is observed after the treatment of spheroids with the different light sources. For $t_I = 2$ min the fraction of AO stained cells, mainly located at the center of the spheroids, is significantly larger after illumination with LED A in comparison with the culture treated with LED D. Moreover, the 2D annulus is poorly observed after LED A illumination.

For $t_I = 12$ min, the comparison of both contrast phase and fluorescence images of cultures 24 h post-illumination with LED A indicates that all cells from the 3D colony core were eliminated. Moreover, the 2D annulus of live cells before illumination (figure 6(c), left column) goes away (for LED D) or appears necrotic after PDT treatment (for LED A).

The results presented in this section are consistent with figure 4 of MTT viability and TUNEL assays of HeLa cell monolayers, hinting at a more effective PDT outcome for the violet light.

3.2.2. *Colony dynamics to evaluate PDT treatment*

In previous works we reported on the dynamics of 2D and 3D regions of large quasi-circular cell colonies originated by cell spheroids (Huergo *et al* 2011, 2014) to infer about the colony expansion process. In the present case, employing either LED A or LED D, we compare the effect of PDT by following both the 2D and 3D colony growth.

After their adhesion, cell spheroids were incubated with the photosensitizer at concentration $C_p = 2\ \mu g\ ml^{-1}$ for 24 h before PDT treatment with the desired LED light. The follow-up of colonies started about 12 h after the spheroid adhesion to the bottom of the Petri dish (t_0). Thus, in most of the cases as indicated above, colonies were formed by a central core of 3D cell agglomerate and an annulus region 1–4 cells thick of 2D growth. Images of the colony pattern were obtained 12 h after cell aggregate adhesion, immediately after illumination, at 2, 5 and 9 h after illumination and daily for about a week (figures 7(a)–(c)).

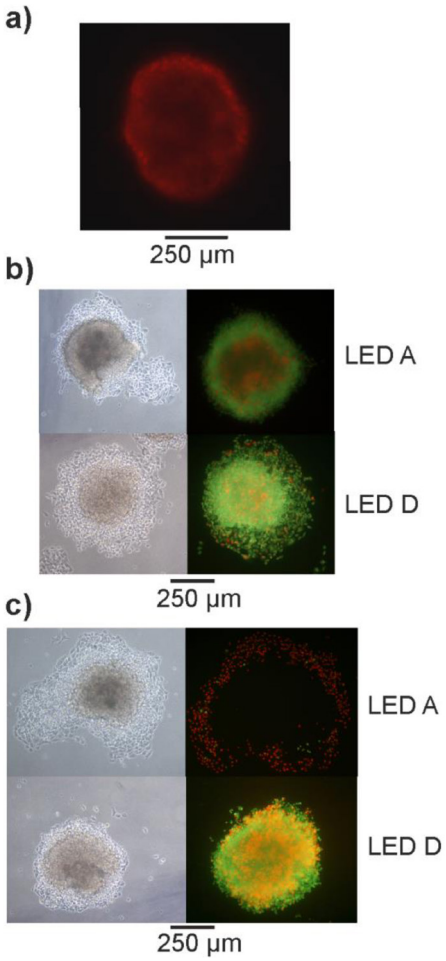

Figure 6. (a) Fluorescence of m-THPC from a typical cell spheroid before illumination. (b) and (c) Typical cell spheroids after illumination with LED A and LED D; (b) $t_I = 2$ min; (c) $t_I = 12$ min. Spheroids were incubated with $C_p = 1\ \mu g\ ml^{-1}$ for 24 h. Left: contrast phase images of spheroids before incorporation of the drug. Right: fluorescence images of AO/PI stained spheroids 24 h post-illumination with light of LEDs indicated in the figure.

Results from untreated cultures (without incubation with the photosensitizer and without illumination) were in agreement with those obtained previously for a different cell line (Huergo *et al* 2014). The average 2D cell colony radius follows a linear relationship with the growth time. Data from the 2D colony expansion for untreated and illuminated colonies are depicted in figures 8(a)–(c). Before illumination, the average colony radius increases with t; then 2 h post-illumination the colony growth expansion velocity becomes negative. Subsequently, the expansion velocity attains a minimum value at 30–50 h, and afterwards it increases. Cultures treated with LED A exhibit a more noticeable decrease in the average colony radius in comparison with cultures illuminated with LED D. Furthermore, for LED A the increase in the displacement velocity after the 'quiescent regime' tends to diminish with t approaching a constant value. This fact is absent for untreated cultures and those illuminated with LED D (figures 8(a) and (b)).

The 3D core evolution was evaluated by following the average radius of the hand-traced contours after setting the appropriate image contrast level. Data indicate a similar behavior to that given for 2D culture annular regions of untreated and PDT treated cultures, although some distinct characteristics can be pointed out. The average radius of the 3D core 2 h after illumination exhibits an increase, in the case of cultures illuminated with LED D, and a relatively small decrease for cultures illuminated with LED A. This behavior contrasts with that of the 2D colony region average radius. For the latter, the average radius decreases almost immediately after illumination (figures 8(b) and (c)). It is worth noting that the increase observed for the 3D colony core of LED D PDT treated cultures is absent in the case of untreated spheroids. These results are in agreement with the deeper penetration of LED D light in comparison to that of LED A, the former achieving a more effective PDT treatment outcome at the deeper cell layers, producing a larger number of dead cells that would go to the 3D aggregate and remain transitorily increasing its average radius.

Confocal image data will give further insight about the PDT outcome for the different light sources employed, as described in the next section.

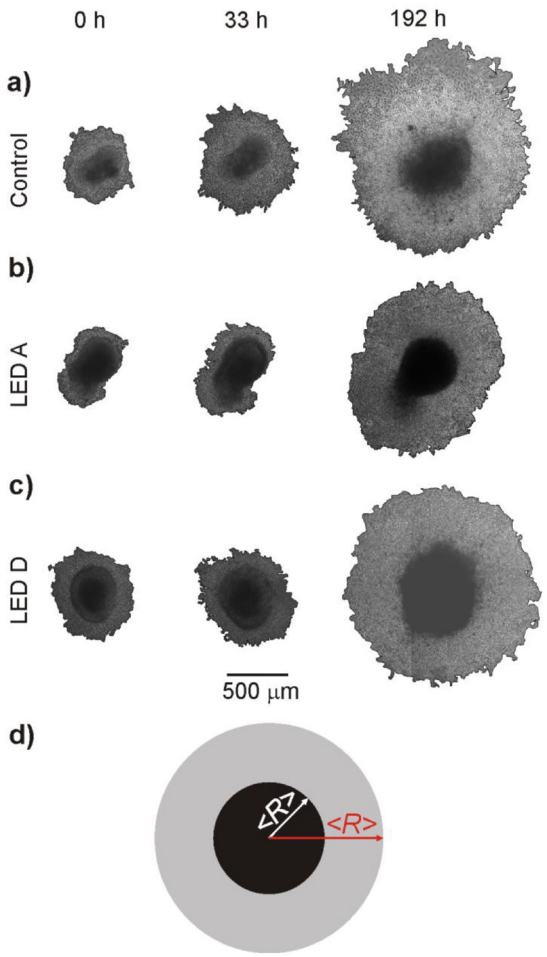

Figure 7. Contrast phase images of the evolution of HeLa cell colony patterns. (a) An untreated culture; (b) treated culture for $t_I = 8$ min with LED A; (c) treated culture for $t_I = 8$ min with LED D. Cultures were incubated with $C_p = 2\ \mu g\ ml^{-1}$ for 24 h; (d) scheme of an adhered spheroid. The average radii of the central core and that of the 2D culture region are depicted. The scale bar is included.

3.2.3. *Confocal images of HeLa cell spheroids after PDT treatment*

Fluorescence confocal images of AO and PI stained cells in spheroids (figure 9) show the effect of PDT treatment on 3D HeLa cell cultures. Results from untreated spheroids are compared to spheroids incubated with 2 μg ml^{-1} m-THPC for 3 h and illuminated with LED A for $t_I = 4$ min and observed at 3–5 h post-illumination (figure 9). This observation time is appropriate as dynamic data presented in the previous section indicate that no significant changes in colony cell pattern are observed.

AO and PI staining of an untreated (figure 9(a)) and PDT treated spheroid (figure 9(b)) shows a green fluorescence coming from live cells with a rather deep inner region, and orange highlighted regions (stained with PI) close to the center of the spheroid that are mainly composed of dead cells. For the untreated spheroid, the amount of dead cells is very small and only a few cells located at inner regions stained with PI can be seen. This fact is more clearly distinguished from the pie plots depicted in the figure. For the treated HeLa cell spheroids employing LED A, the PDT effect, quantified as the amount of PI stained cells, can be distinguished (figure 9(b)) from the fluorescence images at different distances from the spheroid apex (d) and the corresponding pie plots. The outermost layers are highlighted in bright green (stained with AO) and consist of proliferative cells. After illumination this staining pattern may appear contradictory, but it can be understood considering the dynamic data from cell colonies that indicate a reorganization involving the transfer of damaged cells from the basal plane to the 3D regions. Subsequently, dead cells at the periphery would be detached from the spheroid.

These results suggest that PDT experiments with spheroids can be used to evaluate the extension of the PDT treatment in relation mainly to the photosensitizer concentration and the amount of light deposited on different sections of the sample. We intend to advance a semiquantitative correlation between these factors and the PDT outcome at different sections of the spheroid. More data and further analysis would be required to set this type of experiment as models for improving strategies for PDT applications.

Data from a set of five similar spheroids for each condition, i.e. treated with light of LED A or with light of LED D, are represented as the fraction of AO/PI stained cells as a function of the depth (d), measured from

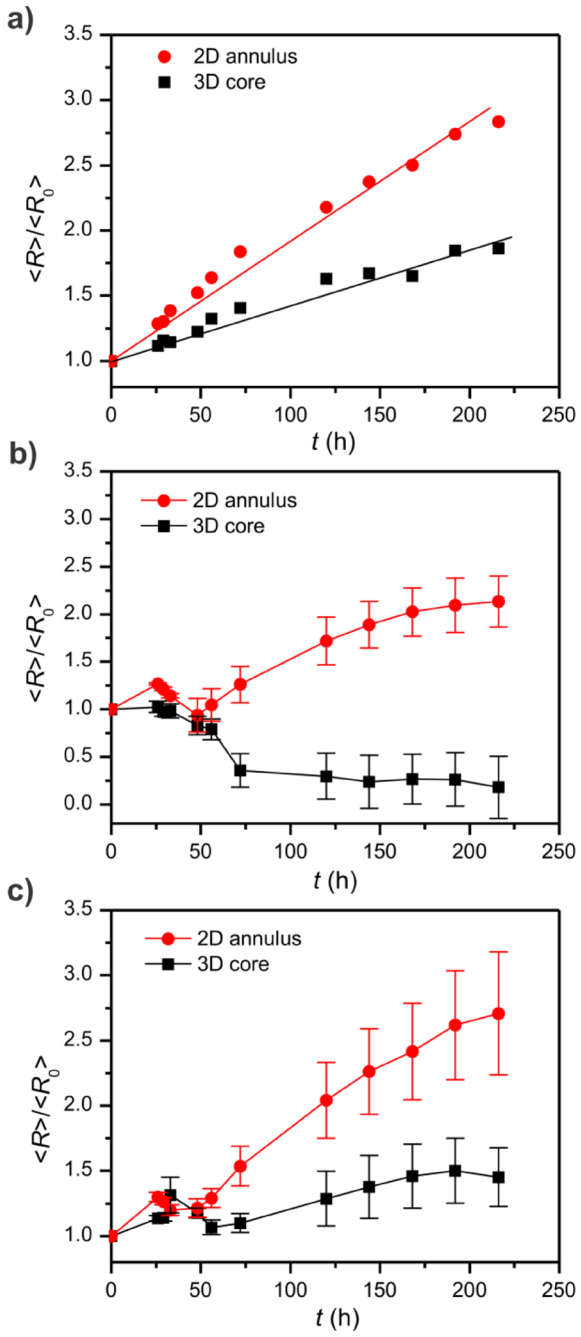

Figure 8. 2D and 3D HeLa cell colony dynamics. (a) Untreated spheroids with neither drug nor illumination; (b) spheroids illuminated with LED A for $t_i = 8$ min; (c) spheroids illuminated with LED D for $t_i = 8$ min. Spheroids were incubated with m-THPC at $C_p = 2\ \mu g\ ml^{-1}$ for 24 h.

the apex of the spheroid to the basal plane (figures 9 and 10(a)). The above-mentioned tendency is confirmed although the analysis of each section involves a large measurement error. Despite this drawback, it can be seen that the illumination with LED A induces a larger fraction of PI stained dead cells than the illumination with LED D. The PDT effect of both light sources decreases with d, although this tendency is more pronounced for the violet light. At deeper planes the PDT effect of LED A is similar to or tends to be even smaller than that of LED D.

The proportion of surviving HeLa cells (figure 10(b)), obtained from the proportion of dead cells (figure 10(a)), at each section along the thickness of the spheroid, decreases in going from the apex of the spheroid to its basal plane. LED A and LED D light is attenuated differently through the cell spheroid.

The representation of the survival fraction of cells as a function of $1/d$ (figure 10(b)) exhibits a similar form to that reported in the literature for studies employing a suspension of MLL cells (Dysart and Patterson 2005). In the present work the fluence is affected by the penetration of light through the spheroid. Accordingly, the photodynamic dose would increase with the fluence following a logarithmic dependence, and the attenuation of the fluence increases with the distance. The effective attenuation is strongly influenced by scattering. Thus an

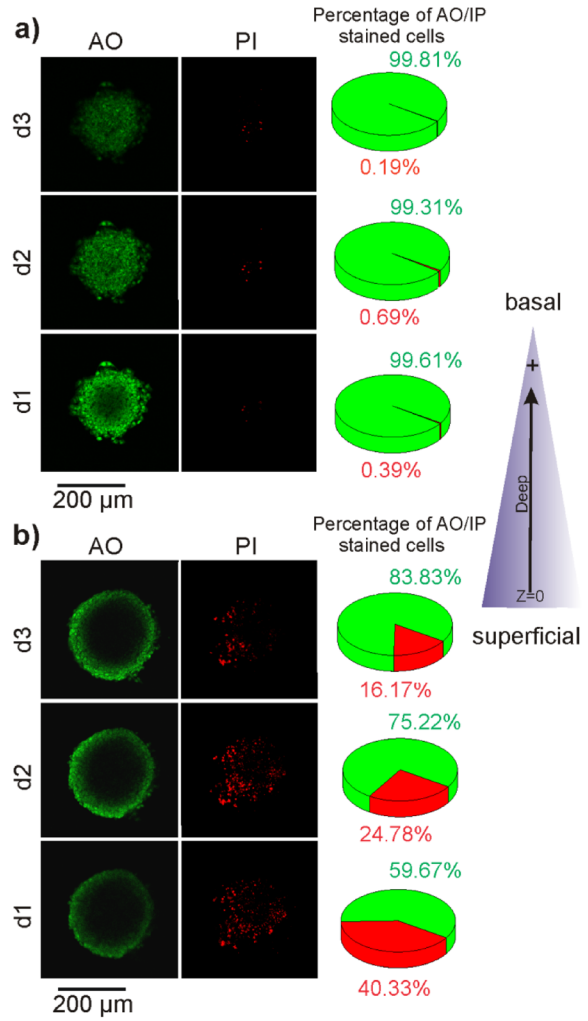

Figure 9. (a) Fluorescence images of AO and PI staining of untreated HeLa cell spheroid. (b) AO and PI stained cells form PDT treated HeLa cell spheroid employing LED A with $t_I = 4$ min. The images were taken with the following depth values: d1 = 20, d2 = 50 and d3 = 100 μm. Pie plots of the relative percentage of AO/PI staining from the untreated and PDT treated spheroids are included for each image. Images were taken 3 h after illumination from cultures that had been previously incubated with 2 μg ml^{-1} m-THPC for 3 h. The scale bars and the increasing depth in the spheroids as well as the light intensity gradient are indicated in the figure.

approximate description of the survival fraction of cells with the inverse of the distance from the spheroid apex could be given employing an equation similar to that given in from Dysart and Patterson (2005):

$$\text{Survival fraction} = 1 - (1 - \exp(-D/D_0))^u. \quad (2)$$

With D/D_0 being the fraction of PDT dosage, in this case related to the relative fluence arriving at each section of the cell spheroid that decreases with the d, and u a constant related to the shoulder of the survival curve (Ma *et al* 2007). Although we are not able to measure the PDT dose, equation (2) is used to fit data to quantify the differences between deep red and violet LED lights.

A reasonable coincidence is observed (solid and dotted traces in figure 10(b)) between experimental data and the theoretical expression. Data would be dispersed mainly by the influence of the heterogeneously distributed photosensitizer, in particular if data from the spheroid periphery are considered. Despite this drawback, fitting traced curves allows confirming the differences between the LED sources employed in the present work: a more effective PDT outcome for LED A compared to LED D, which can be better noticed at the upper sections of cell spheroids, and a faster increase in the fraction of surviving cells for LED A. Fluence variation is larger for LED A than for LED D, thus u from equation (2) results larger for the former than for the latter.

4. Discussion

The increased photodynamic reaction efficiency for light in the 400–430 nm range has been proposed to be useful for PDT applications on superficial tumors (Moan *et al* 1989). More recently it has been reported that the PDT treatment employing a blue LED light source is more effective than red light in the 630–660 nm range

when δ-aminolevulinic acid or its derivatives (Hatakeyama *et al* 2013, Helander *et al* 2014), photofrin (Moan and Sommer 1984), or even natural photosensitizers (Jamali *et al* 2018) are utilized. In another research work, for melanotic melanomas, PDT with aminolevulinic acid and the combination of violet light of 420 nm wavelength with red light improved the PDT outcome (Ma *et al* 2007). These facts are explained by the 20–30-fold larger absorption of the Soret band in comparison with bands in the red spectrum region of the photosensitizer dissolved in phosphate buffer. Recently, a wireless photonic miniaturized implantable device for the delivery of violet and red light for PDT applications has been proposed (Bansal *et al* 2018), thus expanding the possibilities of PDT.

In our work, we utilize m-THPC as photosensitizer, and according to the MTT and TUNEL assay results, the above-mentioned behavior is supported by our violet light (section 3.1). Then we use HeLa cell spheroids to confirm this trend and demonstrate the usefulness of violet light (LED A) compared with deep red light (LED D) (Section 3.2).

The most common photosensitizers utilized in PDT exhibit absorption bands in both the violet and red spectrum regions. However, it is worth noting that the absorption band is the largest for the violet region, as in the case of m-THPC (figure 2). This is an important fact for possible applications of violet light in the treatment of early cases of cervical uterine carcinoma.

The overlapping of the emission of LED A with the m-THPC absorption spectra, as well the excitation-fluorescence spectrum of m-THPC bound to cells, is larger than for the other LED sources employed in our work. A similar excitation-fluorescence spectrum for m-THPC bound to V-79 (Chinese hamster lung fibroblast) and its resemblance to the action spectrum have been reported (Ma *et al* 1994). From Tunnel data it is possible to infer that both LED A and LED D light wavelengths induce the same type of cell death, at least within our experimental errors. In fact, the type of cell death would depend on several factors as reviewed in the Introduction Section and other research papers (Yoo and Ha 2012).

Although the PDT treatment outcome of cell monolayer cultures is more effective for LED A, the smaller light penetration for wavelength approaching violet than red should be considered. For any possible applications of violet light in the treatment of early cases of cervical uterine carcinoma, the light must be capable of traversing about 300 μm, the average thickness of the cervical epithelium (figure 2). The utilization of 3D models for studying the photodynamic dose has recently been reviewed (Mohammad-Hadi *et al* 2018), representing a valuable alternative to animal models. Thus, several mathematical equations have been proposed for quantification of the PDT dose and to infer the PDT outcome in different multicellular systems, including suspension of cells and spheroids (Finlay *et al* 2004, Dysart and Patterson 2005, Dysart *et al* 2005, Dysart and Patterson 2006). They incorporate the experimental fluorescence measurement during the treatment as well as the photobleaching of the photosensitizer, and the determination of singlet oxygen that is used as a universal measurement of the dose (Dysart and Patterson 2006). The bleaching of Photofrin in multicell tumor spheroids has also been interpreted by a mathematical model, in which the reactions of singlet oxygen with the photosensitizer, and the reactions between the photosensitizer triplet and biological targets are considered (Finlay *et al* 2004). Furthermore, improved models include the experimental support of spectroscopic determination of products at different conditions (Dysart and Patterson 2006).

On the other hand, the study of the cell colony growth has been proposed to be useful to infer about physiological and pathological processes in the organism in which those cells are involved (Brú *et al* 2003). The dynamics of both 2D and 3D colonies generated by spheroids and followed by measuring the evolution of the average radius of either the 3D core or the 2D annulus region exhibited distinctive pattern evolution reflecting the PDT treatment outcome for LED A and LED D. Furthermore, these experiments allow the choice of the proper observation time to evaluate AO/PI stained cells at the different sections of 3D spheroids. Thus, one of the goals of this work was to utilize 3D spheroids to infer the PDT dose for both violet and red light at low fluence rate at different sections of the spheroid. It appears that PDT treatment outcome for the violet light was more effective than the red light at the upper sections of the spheroids up to about 100 μm, and the overall effectiveness was higher even for spheroids about 300 μm in diameter. This size is close to the distance the light is required to penetrate for the treatment of superficial neoplastic cervical lesions. Furthermore, the PDT outcome (cell survival fraction) as a function of 1/d is reasonably well described as suggested in the literature for a cell suspension (Dysart and Patterson 2005). Nevertheless, this type of correlation requires more research work to support the use of spheroids as a light dosage model.

It has been indicated that PDT treatment with light wavelengths different than red has been reported to be convenient for the treatment of rather superficial tumors (Fritsch *et al* 1997, Grosjean *et al* 1998, Dijkstra *et al* 2001, Maytin *et al* 2018). It has been also reported that Photofrin II and green light were effective in the eradication of esophagus intramucosal carcinoma. This tumor is usually flat, and although green light penetration is smaller than red light, a higher absorption of green light by Photofrin II makes the treatment more selective, reducing the risk of perforation (Jacques 2013). Moreover, the higher efficiency of δ-aminolevulinic acid-based PDT with violet light in comparison with red light has been appreciated in the treatment of dermatologic

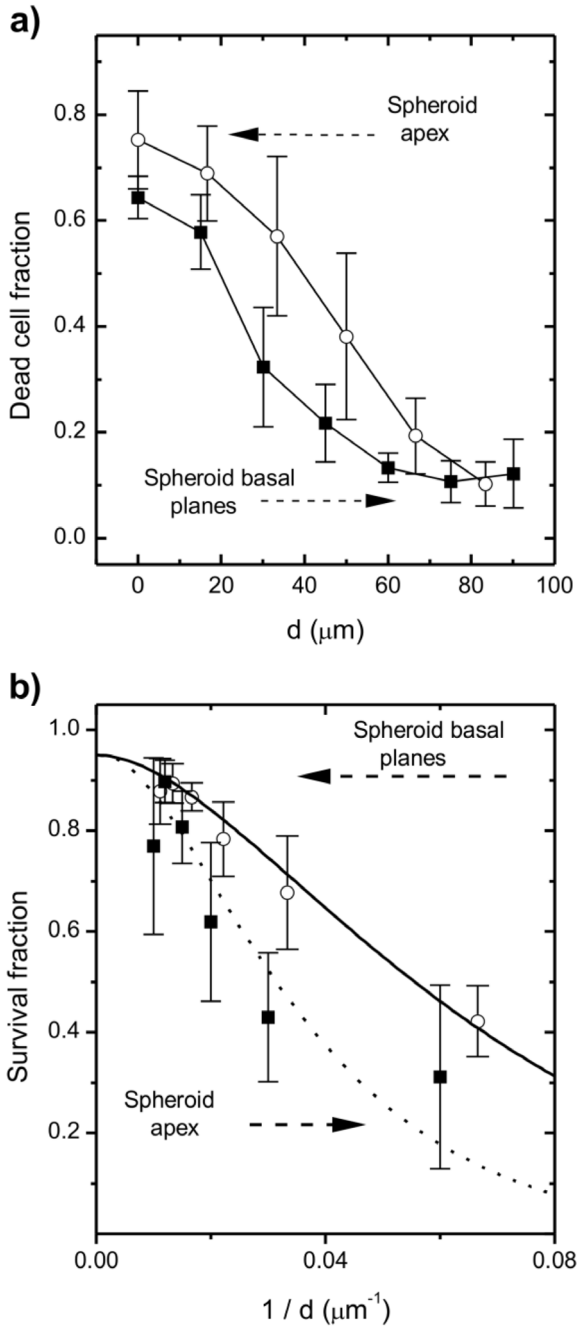

Figure 10. Effect of PDT treatment on different planes of HeLa cell spheroids determined from AO/PI stained confocal fluorescence images. (a) Fraction of dead cells versus depth (d) measured from the apex of the spheroids illuminated for 8 min with LED D (black squares) and LED A (open circles). (b) The average fraction of surviving cells as a function of $1/d$ (the fluence decreases in going from the spheroid apex to the basal plane). The standard error is included for $n = 5$. Solid and dotted traces are representations of equation (2) with $u = 2.0$ and $u = 0.22$, for LED A and D, respectively. Cell spheroids were incubated with 2 μg ml^{-1} m-THPC for 3 h before the PDT treatment.

diseases such as actinic keratosis, Bowen's disease and basal cell carcinoma (Dijkstra *et al* 2001). More recently, the treatment for basal cell carcinoma in patients with basal cell nevus syndrome with 400 nm light has been reported to be as effective as PDT with red light (Maytin *et al* 2018). In this case, treatments were administered in three biweekly sessions during four months, as a safety feature.

Finally, the local PDT for women with CIN 1/2, performed with the intravaginal administration of hexaminolevulinate and red light from a LED-based device, has been reported (Hillemmans *et al* 2015). The authors concluded that PDT appears to be promising for the treatment of women with clinically relevant CIN and persistent oncogenic HPV infections.

The results presented in our work intend to contribute to the expansion of PDT with violet light, particularly in the treatment of low grade CINs exhibiting a superficial dysplasia and profiting from of the high absorption coefficient of most of the photosensitizers employed.

5. Conclusions

In this work we present results of PDT performed in both 2D and 3D HeLa cell cultures employing m-THPC as photosensitizer and LED light of different wavelengths: violet, blue, red, and deep red. Viability data indicate that the most effective light source is LED A (violet), followed by LED D (deep red). The dynamics of both 2D and 3D regions of the cell spheroids, which were followed up for about 7 d, render complementary data about the outcome of the treatment with either LED A or LED D and allow the choice of the most appropriate conditions for performing confocal fluorescence observations.

The comparison of confocal microscopy data from PDT experiments performed employing LED A and D for illuminating HeLa cell spheroids 80–300 μm in diameter reveals that, although there is a deeper penetration of the red light, the larger absorption of m-THPC in the violet region makes this light sufficiently effective.

It is important to emphasize that the results in the present work support the utilization of violet LED light to treat the early stages of neoplastic cervical diseases.

Acknowledgments

The authors thank Dr H Poteca for providing the photosensitizer, Eng. Aníbal Laquidara, Dr Fausto Bredice, and Eng. Pablo Ixtaina for their electronic, spectrometric and photometric-radiometric contributions, respectively. This work received the financial support from CONICET (PIP 0602) and the Universidad Nacional de La Plata grants through Facultad de Ciencias Médicas and Facultad de Ingeniería, and the Fundación Innovatec, Argentina. MAP is a staff members of CONICET and MG is Professor Emeritus of UNLP.

ORCID iDs

Miguel A Pasquale https://orcid.org/0000-0002-0416-100X

References

Abrahamse H and Hamblin M R 2016 New photosensitizer for photodynamic therapy *Biochem. J.* **473** 347–64
Agarwal M L, Clay M E, Harvey E J, Evans H H, Antúnez A R and Oleinick N L 1991 Photodynamic therapy induces rapid cell death by apoptosis in L5178Y mouse lymphoma cells *Cancer Res.* **51** 5993–6 (PMID:1933862)
Allison R R and Moghissi K 2013 Oncologic photodynamic therapy: clinical strategies that modulate mechanisms of action *Photodiagnosis Photody. Ther.* **10** 331–41
Allison R R, Bagnato V S and Sibata C H 2010 Future of oncologic photodynamic therapy *Future Oncol.* **6** 929–40
Angell-Petersen E, Spetalen S, Madsen J S, C-H Sun, Peng Q, Carper S W, Sioud M and Hirschberg H 2006 Influence of light fluence rate on the effects of photodynamic therapy in an orthotopic rat glioma model *J. Neurosurg.* **104** 109–17
Ash C, Dubec M, Donne K and Bashford T 2017 Effect of wavelength and beamwidth on penetration in light-tissue interaction using computational methods *Laser Med. Sci.* **32** 1909–18
Babilas P, Kohl E, Maisch T, Bäcker H, Groß B, Branzan A L, Bäumler W, Landthaler M, Karrer S and Szeimies R M 2006 *In vitro* and *in vivo* comparison of two different light sources for topical photodynamic therapy *Br. J. Dermatol.* **154** 712–8
Bansal A, Yang F, Xi T, Zhang Y and Ho J S 2018 *In vivo* wireless photonic photodynamic therapy *Proc. Natl Acad. Sci. USA* **115** 1469–74
Baran T M and Foster T H 2012 Fluence rate dependent photobleaching of intratumorally administered Pc 4 does not predict tumor growth delay *Photochem. Photobiol.* **88** 1273–9
Bonnett R, White R D, Winfield U-S and Berenbaum M C 1989 Hydroporphyrins of the meso-tetra(hydroxyphenyl)porphyrin series as tumor photosensitizers *Biochem. J.* **261** 277–80
Boyle D G and Potter W R 1987 Photobleaching of photofrin II as a means of eliminating skin photosensitivity *Photochem. Photobiol.* **46** 997–1001
Brenner D J, Hlatky V, Hahnfeldt P, Huang Y and Sachs R K 1998 The linear-quadratic model and most other common radiobiological models result in similar predictions of time-dose relationships *Radiat. Res.* **150** 83–91
Brú A, Albertos S, Subiza J L, García-Asenjo J L and Brú I 2003 The universal dynamics of tumor growth *Biophys. J.* **85** 2948–61
Castano A P, Demidova T N and Hamblin M R 2005 Mechanism in photodynamic therapy: part three—photosensitizer pharmacokinetics, biodistribution, tumor localization and mode of tumor destruction *Photodiagnosis Photodyn. Ther.* **2** 91–106
Dias Ribeiro A P, Pavarina A C, Zardo Trindade F, Mayumi Inada N, Bagnato V S and de Souza Costa C A 2010 Photodynamic therapy associating Photogem^{R} and blue LED on L929 and MDPC-23 cell culture *Cell Biol. Int.* **34** 343–51
Dijkstra A T, Majoie I M L, Van Dongen J W F, Van Weelden H and Van Vloten W A 2001 Photodynamic therapy with violet light and topical 6-aminolaevulinic acid in the treatment of actinic keratosis, Bowen's disease and basal cell carcinoma *J. Eur. Acad. Dermatol. Venereol.* **15** 550–4
Dougherty T J, Gomer C J, Henderson B W, Jori G, Kessel D, Korbelik M, Moan J and Peng Q 1998 Photodynamic therapy *J. Natl. Cancer Inst.* **90** 889–905
Dubessy C, Merlin J-L, Marchal C and Guillemin F 2000 Spheroids in radiobiology and photodynamic therapy *Crit. Rev. Oncol. Hemat.* **36** 179–92
Dysart J S and Patterson M S 2005 Characterization of Photofrin photobleaching for singlet oxygen dose estimation during photodynamic therapy of MLL cells *in vitro Phys. Med. Biol.* **50** 2597–616
Dysart J S and Patterson M S 2006 Photobleaching kinetics, photoproduct formation, and dose estimation during ALA induced PpIX PDT of MLL cells under well oxygenated and hypoxic conditions *Photochem. Photobiol. Sci.* **5** 73–81

Dysart J S, Singh G and Patterson M S 2005 Calculation of singlet oxygen dose from photosensitizer fluorescence and photobleaching during m-THPC photodynamic therapy of MLL cells *Photochem. Photobiol.* **81** 196–205
Enk C D and Levi A 2012 Low-irradiance red LED traffic lamps as light sources in PDT for actinic keratoses *Photodermatol. Photoimmunol. Photomed.* **28** 332–4
Etcheverry M E, Pasquale M A, Gutiérrez A, Bibé S, Ponzinibbio C, Poteca H and Garavaglia M 2018 Photodynamic therapy in fibrosarcoma BALB/c animal model: Observation of the rebound effect *Phothodiagnosis Phothodyn. Ther.* **21** 98–107
Evans C L 2015 Three-dimensional *in vitro* spheroid models for photodynamic therapy: strengths and opportunities *Frontiers Phys.* **3**
Finlay J C and Darafsheh A 2016 Light sources, drugs, and dositometry *Biomedical Optics in Otorhinolaryngology: Head and Neck Surgery* ed B Wang and J Ilgner (New York: Springer)
Finlay J C, Mitra S, Patterson M S and Foster T H 2004 Photobleaching kinetics of Photofrin *in vivo* and in multicell tumour spheroids indicate two simultaneous bleaching mechanisms *Phys. Med. Biol.* **49** 4837–60
Foster T H, Hartley D F, Nichols M G and Hilf R 1993 Fluence rate effects in photodynamic therapy of multicell tumor spheroids *Cancer Res.* **53** 1249–54 (PMID:8443805)
Fritsch C, Stege H, Saalmann G, Goerz G, Ruzicka T and Krutmann J 1997 Green light is effective and less painful than red light in photodynamic therapy of facial solar keratosis *Photodermatol. Photoimmunol. Photomed.* **13** 181–5
Gaio E, Scheglmann D, Reddi E and Moret F 2016 Uptake and photo-toxicity of Foscan^{R}, Foslip^{R} and Fospeg^{R} in multicellular tumor spheroids *J. Photochem. Photobiol.* B **161** 244–52
Ghosh I, Mittal S, Banerjee D, Chowdhury N and Basu P 2015 Study of correlation of cervical epithelial thickness with the grade of colposcopic abnormality *Int. J. Gynecol. Pathol.* **35** 269–74
Grosjean P, Wagnieres G, Fontolliet C, van den Bergh H and Monnier P 1998 Clinical photodynamic therapy for superficial cancer in the oesophagus and the bronchi: 514 nm compared with 630 nm light irradiation after sensitization with Photofrin II *Br. J. Cancer* **77** 1989–95
Hartl B A, Hirschberg H, Marcu L and Cherry S R 2015 Characterizing low fluence thresholds for *in vitro* photodynamic therapy *OSA Biomed. Opt. Express* **6** 770–9
Hatakeyama T *et al* 2013 Efficacy of 5-aminolevulinic acid-mediated photodynamic therapy using light-emitting diodes in human colon cancer cells *Oncol. Rep.* **29** 911–6
Helander L, Krokan H E, Johnsson A, Gederaas O A and Plaetzer K 2014 Red versus blue light illumination in hexyl 5-aminole vulinate photodynamic therapy: the influence of light color and irradiance on the treatment outcome *in vitro J. Biomed. Opt.* **19** 088002
Hillemmans P, Garcia F, Petri K U, Dvorak V, Sadovsky O, Iversen O-E and Einstein M H 2015 A randomized study of hexaminolevulinate photodynamic therapy in patients with cervical intraepithelial neoplasia 1/2 *Am. J. Obstetr. Gynecol.* **212** 465
Horrobin D F (ed)1994 *New Approaches to Cancer Treatment: Unsaturated Lipids and Photodynamic Therapy* (Great Britain: Churchill Communications Europe)
Huergo M A C, Muzzio N E, Pasquale M A, Bolzán V, González P H and Arvia A J 2014 Dynamic scaling analysis of two-dimensional cell colony fronts in a gel medium: a biological system approaching a quenched Kardar–Parisi–Zhang universality *Phys. Rev.* E **90** 22706
Huergo M A C, Pasquale M A, Bolzán A E, González P H and Arvia A J 2011 Dynamics and morphology characteristics of cell colonies with radially spreading growth fronts *Phys. Rev.* E **84** 021917
Huergo M A C, Pasquale M A, González P H, Bolzán A E and Arvia A J 2012 Growth dynamics of cancer and their comparison with noncancerous cells *Phys. Rev.* E **85** 011918
Jacques S L 2013 Corrigendum: optical properties of biological tissues: a review *Phys. Med. Biol.* **58** R37–61
Jamali Z, Marjaneh Hejazi S, Mohsen Ebrahimi S, Moradi-Sardareh H and Paknejad M 2018 Effects of LED-Based photodynamic therapy using red and blue lights, with natural hydrophobic photosensitizers on human glioma cell line T *Photodiagnosis Photodyn. Ther.* **21** 50–4
Jarvi M T, Patterson M S and Wilson B C 2012 Insights into photodynamic therapy dosimetry: simultaneous singlet oxygen luminescence and photosensitizer photobleaching measurements *Biophys. J.* **102** 661–71
Lacowicz J R 2006 *Principle of Fluorescence* 3rd edn (Singapore: Springer)
Lorenz K J and Maier H 2009 Photodynamic therapy with meta-tetrahydroxyphenylchlorin (Foscan®) in the management of squamous cell carcinoma of the head and neck: experience with 35 patients2009 *Eur. Arch. Otorhinolaryngol.* **266** 1937–44
Ma L, Moan J and Berg K 1994 Evaluation of a new photosensitizer, meso-tetra-hydrohyphenyl-chlorin, for use in photodynamic therapy: a comparison of its photobiological properties with those of two other photosensitizers *Int. J. Cancer* **57** 883–8
Ma L-W, Nielsen K P, Iani V and Moan J 2007 A new method for photodynamic therapy of melanotic melanoma—effects of depigmentation with violet light photodynamic therapy *J. Environ. Pathol. Toxicol. Oncol.* **26** 165–72
Madsen S J, Sun C-H, Tromberg B J, Cristini V, De Magalhares N and Hirshberg H 2006 Multicell tumor spheroids in photodynamic therapy *Laser Surg. Med.* **38** 555–64
Martínez Abaunza V E, Mendoza Castellanos A, Uribe Pérez C J and García Ayala E 2005 Computational model for squamous cells characterization during cervical smear cytology *Rev. Colomb. Biotecnol.* **7** 35–46
Maytin E V, Kaw U, Ilyas M, Mack J A and Hu B 2018 Blue light versus red light for photodynamic therapy of basal cell carcinoma in patients with Gorlin syndrome: a bilaterally controlled comparison study *Photodiagn. Photodyn. Ther.* **22** 7–13
Moan J and Sommer S 1984 Action spectra for hematoporphyrin derivative and Photofrin II with respect to sensitization of human cells *in vitro* to photoinactivation *Photochem. Photobiol.* **40** 631–4
Moan J, Berg V, Bommer J C and Western A 1992 Action spectra of phthalocyanines with respect to photosensitization of cells *Photochem. Photobiol.* **56** 171–5
Moan J, Iani V and Ma L 1989 Choice of the proper wavelength for photochemotherapy *Proc. SPIE* **2625** 544–9
Mohammad-Hadi L, MacRobert A J, Loizidou M and Yaghini E 2018 Photodynamic therapy in 3D cancer models and the utilization of nanodelivery syatems *Nanoscale* **10** 1570–81
Morales Cruzado B and Vázquez-Montiel S 2011 Obtención de los parámetros ópticos de la piel usando algoritmos genéticos y MCML *Rev. Mex. Fis.* **57** 375–81
Muzzio N E, Pasquale M A, González P H and Arvia A J 2014 Influence of individual cell motility on the 2D front roughness dynamics of tumor cell colonies *J. Biol. Phys.* **40** 285–308
Nonaka T, Nanashima A, Nonaka M, Uehara M, Isomoto H, Asahina I and Nagayasu T 2010 Analysis of apoptotic effects induced by photodynamic therapy in a human biliary cancer cell line *Anticancer Res.* **30** 2113–8 (PMID:20651359)
Novak B, Peteja M, Brueck T and Luebbert H 2016 Potency of different red light sources in photodynamic induction of cell death in a squamous cell carcinoma cell line *Photodiagnosis Photodyn. Ther.* **14** 128–30
Oleinick N L and Evans H H 1998 The photobiology of photodynamic therapy: cellular targets and mechanisms *Radiat. Res.* **150** S146–56 (PMID:9806617)

Penjweini R, Kim M M, Finlay J C and Zhu T C 2016 Investigating the impact of oxygen concentration and blood flow variation on photodynamic therapy *Proc. SPIE* **9694** 96940L
Pereira P M R, Berisha N, Bhupathiaraju N V S D K, Fernandes R, Tomé J P and Drain C M 2017 Cancer cell spheroids are better screen for the photodynamic efficiency of glycosylated photosensitizers *PLoS One* **12** e0177737
Potter W R 1986 The theory of photodynamic therapy dosimetry: consequences of photodestruction of sensitizer *Proc. SPIE* **712** 124–9
Sandell J L and Zhu T C 2011 A review of *in vivo* optical properties of human tissues and its impact on PDT *J. Biophotonics* **4** 773–87
Senge M O and Brandt J C 2011 Temoporfin (Foscan, 5,10,15,20-tetra(m-hydroxyphenyl)chlorin)—a second-generation photosensitizer *Photochem. Photobiol.* **87** 1240–96
van de Hulst H C 1980 *Multiple Light Scattering* (New York: Academic)
Walhoomers J M M, Jacobs M V, Manos M M, Bosch F X, Kunmer J A, Shah K V, Snijders P J F, Peto J, Meijer J L M and Muñoz M 1999 Human papillomavirus is a necessary cause of invasive cervical cancer worldwide *J. Pathol.* **189** 12–9
Wilson B C and Patterson M S 2008 The physics, biophysics and technology of photodynamic therapy *Phys. Med. Biol.* **53** R61–109
World Health Organization 2014 *Comprehensive Cervical Cancer Control: a Guide to Essential Practice* 2nd edn (Switzerland: WHO Press)
Yoo J O and Ha K-S 2012 New insights into the mechanisms for photodynamic therapy-induced cancer cell death *Int. Rer. Cell. Mol. Biol.* **295** 139–74